

Flexural behavior and a modified prediction of deflection of concrete beam reinforced with ribbed GFRP bars

Minkwan Ju^{1a}, Cheolwoo Park^{*2} and Yongjae Kim^{2b}

¹Department of Civil and Environmental Engineering, Yonsei University, 50 Yonsei-ro, Seodaemun-gu, Seoul, 03722, Republic of Korea

²Department of Civil Engineering, Kangwon National University, 346 Joongang-ro, Samcheok-si, Kangwon, 25913, Republic of Korea

(Received July 11, 2016, Revised February 10, 2017, Accepted February 12, 2017)

Abstract. This study experimentally investigated the flexural capacity of a concrete beam reinforced with a newly developed GFRP bar that overcomes the lower modulus of elasticity and bond strength compared to a steel bar. The GFRP bar was fabricated by thermosetting a braided pultrusion process to form the outer fiber ribs. The mechanical properties of the modulus of elasticity and bond strength were enhanced compared with those of commercial GFRP bars. In the four-point bending test results, all specimens failed according to the intended failure mode due to flexural design in compliance with ACI 440.1R-15. The effects of the reinforcement ratio and concrete compressive strength were investigated. Equations from the code were used to predict the deflection, and they overestimated the deflection compared with the experimental results. A modified model using two coefficients was developed to provide much better predictive ability, even when the effective moment of inertia was less than the theoretical I_{cr} . The deformability of the test beams satisfied the specified value of 4.0 in compliance with CSA S6-10. A modified effective moment of inertia with two correction factors was proposed and it could provide much better predictability in prediction even at the effective moment of inertia less than that of theoretical cracked moment of inertia.

Keywords: GFRP bar, modulus of elasticity, modified prediction of deflection, effective moment of inertia, proposed model, deformability

1. Introduction

Corrosion of steel reinforcement rapidly deteriorates the structural durability of a reinforced concrete (RC) member during its service life. Corrosion is caused by chloride attack, which can occur through the use of deicing salt and long-term exposure from weathering and a chemical environment. This problem strains the maintenance budget because of the increased number of RC structures that need to be maintained. According to the Federal Highway Administration (FHWA 2010), implementing all potentially cost-beneficial improvements by 2028 under the “improve conditions and performance” scenario would cost approximately 170.1 billion USD per year over 20 years (FHWA 2010). The expensive cycle of maintaining, repairing, and rebuilding infrastructure has led owners to seek more efficient and affordable solutions, such as using fiber-reinforced polymer (FRP) (ISIS Canada 2007). In Korea, the number of structures that need maintenance increased 2.4 times from 2001 to 2011, whereas the cost of the repair and strengthening of bridges significantly increased 8.5 times (ETRI 2013). In order to avoid such

problems, non-corroding reinforcement such as FRP bars has emerged as an alternative to steel reinforcement, and some design specifications address the design and constructing of RC members with FRP bars (AASHTO 2009, ACI 440.1R-15 2015, CAN/CSA S806-12 2012). FRP bars are commercially available in the construction field, and many studies have investigated the flexural capacity of RC members with FRP bars. The flexural strength and serviceability of an RC beam using a smooth glass fiber-reinforced polymer (GFRP) bar with a sand-coated surface have been examined. Various parameters that affect the flexural capacity have been investigated and compared with equations in design codes (Maranan *et al.* 2015). The flexural strength and durability of an RC beam using a GFRP bar wrapped with a helical fiber strand and sand particles attached have been investigated. Using a GFRP bar was found to effectively improve the durability and flexural strength (Wang and Belarbi 2013). Another GFRP bar with indented-shaped ribs was developed in Europe. Barris *et al.* (2009) experimented on the flexural capacity of an RC beam using a GFRP bar with a high modulus of elasticity of around 64.0 GPa. They found that equations in design codes and other formulas predict the performance well in the service limit state, while the load capacity is underestimated at the ultimate limit state. In contrast with steel reinforcement, various FRP bars have different tensile and bond properties. The mechanical properties are usually governed by the fiber volume fraction, which generally ranges from 70% to 87% (<http://www.concrete.org/students/AslanFRPREbar.pdf>; [*Corresponding author, Professor
E-mail: tigerpark@kangwon.ac.kr](http://www.concrete.org/students/Pultrall-V-Rod-Technical-Data-Sheet-for-2009-</p></div><div data-bbox=)

^aResearch Professor
E-mail: j_dean21@naver.com

^bResearch Professor
E-mail: kimseungwok@naver.com

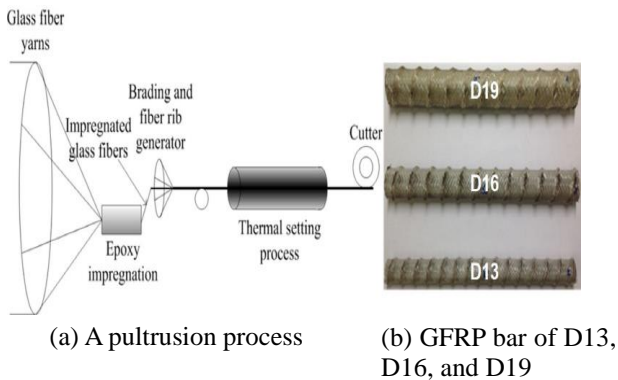


Fig. 1 Ribbed GFRP bars developed in this study

Competition.pdf; Weber 2005). Hence, the tensile properties can be designed according to a deterministic approach.

For the bond properties, however, a deterministic approach is hard to use because concrete is an uncertain material, and the surface characteristics between an FRP bar and concrete can be more vulnerable than those between a steel bar and concrete. Therefore, a sufficient bond strength can effectively transfer the tensile strength of the FRP bar to the concrete member.

This study presents a new ribbed GFRP bar which bond strength is excellently increased as compared to some of commercial GFRP bars. Four point bending test is carried out for concrete beam reinforced with the ribbed GFRP bar. Mode of failure and structural capacity is investigated according to the effect of reinforcing ratio and concrete compressive strength. For ductility evaluation, deformability factor for test beams is calculated and its allowances are investigated. The comparative study is carried out for prediction of deflection by some of code equations and compared with the experiment results. For more accurate prediction of deflection, a modified moment of inertia model is proposed and its predictability is discussed.

2. Experimental program

2.1 Materials

2.1.1 Ribbed GFRP bar

A ribbed GFRP bar was fabricated by the braided pultrusion process (Park *et al.* 2016). It consisted of E-glass fiber and vinyl-ester resin with a designed fiber volume fraction of 78.0%. Fig. 1 shows the GFRP bars used in this study. In order to determine the tensile strength of the GFRP bar, the nominal or measured diameter must be known. To determine the diameter of a smooth bar, ASTM D 3916 (2002) specifies measuring the diameter at several points along the length of the bar. For a ribbed GFRP bar, however, this method is impractical because of the varying cross-sectional dimensions along the bar. A better approach is calculating the average diameter from the mass, length, and density of the bar (Castro and Carino 1998). In this study, the diameter of the GFRP bar specimens was measured by using an immersion test. The weight and

Table 1 Results of measured diameter of ribbed GFRP bar by immersing test

GFRP bar ID	Length (mm)	Unit weight (kgf/m)	Volume (mL)	Density (kg/m ³)	Average diameter (mm)
D13	197.0±1.8	0.270±0.001	27.8±0.4	1913.8±30.8	13.4
D16	197.8±1.5	0.426±0.002	43.0±0.5	1958.8±16.9	16.6
D19	198.0±1.8	0.590±0.004	58.8±2.0	1985.9±66.8	19.4

Table 2 Mechanical properties of the ribbed GFRP bar from You *et al.* (2015)

GFRP bar ID (mm)	Cross sectional area, A_f (mm ²)	Ultimate tensile strength, f_{fu} (MPa)	Guaranteed tensile strength, f_{fu}^c (MPa)	Modulus of elasticity, E_f (GPa)	Ultimate tensile strain, ϵ_{fu} (%)	Guaranteed tensile strain, ϵ_{fu}^c (%)
D13 (13.4) ^a	141.0	1006.5	928.8	56.6	1.79	1.40
D16 (16.6)	216.3	1209.5	1126.1	57.0	2.12	1.31
D19 (19.4)	295.4	882.2	772.3	61.2	1.48	1.25

^avalues of diameter in parentheses are obtained from the immersing test

^baverage ultimate value obtained by tensile test

^caverage ultimate value-3×standard deviation (ACI 440 1R-15)

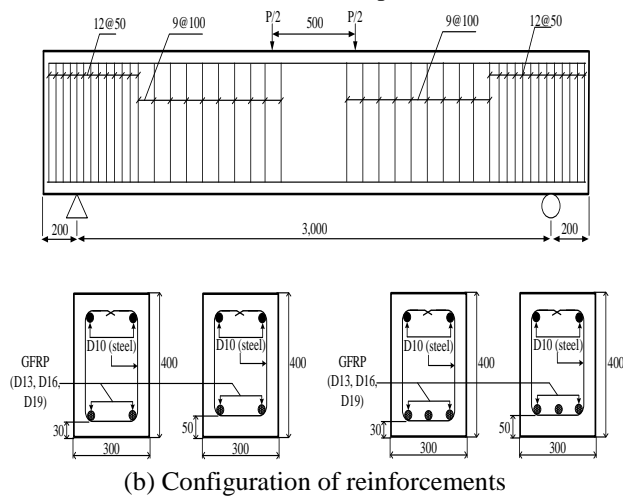
density per unit length of the GFRP bars were measured in a laboratory. The measured lengths ranged from 194 to 202 mm. In total, 13 specimens were tested and averaged. Table 1 summarized the results of measured diameter.

A uniaxial tensile test was carried out on the ribbed GFRP bars by previous research (You *et al.* 2015) in compliance with ASTM D 3916. Table 2 presents the mechanical properties. The cross-sectional area was obtained by using the average diameter from the immersion test. This area is used to determine the tensile strength of the ribbed GFRP bar as reinforcement in the test beams. The average tensile strength and modulus of elasticity were determined by averaging the tensile test results of the specimens, excluding the maximum and minimum values. The modulus of elasticity was determined according to CSA S806-12. The equation uses the applied loads P_1 and P_2 , which correspond to 50% and 25% of the ultimate load, respectively, and ϵ_1 and ϵ_2 , which are the corresponding strains. Strain gauges were installed at $L/2$ for ϵ_1 and $L/4$ for ϵ_2 along the GFRP bar, and the average values were used to determine the tensile strength and modulus of elasticity. The modulus of elasticity was relatively high compared to other commonly used GFRP bars (35-45) reported in previous research (Barris *et al.* 2009). The reduced percent of the guaranteed to ultimate strength was 91% in average, where the strain showed 75% in average. This is because the entire strain was sensitively measured on the glass fiber tissue and epoxy and the alignment of strain gauge might not be fully configured so that it resulted in somewhat high value of the standard deviation. The strain results may provide a conservative structural design of the GFRP reinforced concrete beams.

The bond strength of the GFRP bar in this study was excellent compared to that of widely used existing GFRP bars. According to You *et al.* (2015), the bond strength of ribbed GFRP bars is approximately 42% higher than that of commercial GFRP bars such as Aslan and V-Rod. They



(a) Test set up



(b) Configuration of reinforcements

Fig. 2 Reinforcements and geometry details of the test beams (unit in mm)

found that a GFRP bar can behave uniformly with concrete through a perfect bond, just like steel bars.

2.1.2 Concrete

The used concrete has the specific compressive strength of 30MP obtained by mix design using ordinary Portland cement (OPC). Table 3 summarizes the average compressive strengths. The results of three concrete cylindrical specimens were used for each test beam. Before the experimental test, a compressive test on cylindrical concrete specimens were carried out for the tested beams. Because specific compressive strengths were obtained, a more realistic evaluation of the structural capacity of the test beam was achieved for structural analysis.

2.2 Test specimen

Fig. 2 shows schematics of the test specimens and designed cross-section. All beams were 3400 mm long with a rectangular cross-section of 300×400 mm. The beams were reinforced with ribbed GFRP bars arranged in a single layer in the tension zone. For shear reinforcement, 9.53 mm diameter stirrups were applied with two different kinds of spacing, including a 50 mm spacing along the shear span in

Table 3 Details of test specimens

Beam ID	A_f (mm ²)	f_c (MPa)	ρ_f (%)	ρ_{fb} (%)	ρ_f/ρ_{fb}	
2D13G-C30-1	282.0	42.6	0.266	0.862	0.31	Rupture ^a
2D13G-C30-2		34.0		0.744	0.36	Rupture
2D16G-C30-1	432.6	42.6	0.410	0.612	0.67	Rupture
2D16G-C30-2		25.9		0.423	0.97	Balanced ^b
2D19G-C30-1	590.9	42.6	0.562	1.270	0.44	Rupture
2D19G-C30-2		34.0		1.095	0.51	Rupture
3D13G-C30-1	422.9	42.6	0.398	0.862	0.46	Rupture
3D13G-C30-2		25.9		0.596	0.67	Rupture
3D16G-C30-1	649.0	42.6	0.614	0.423	1.45	Crushing ^c
3D16G-C30-2		34.0		0.528	1.16	Crushing
3D19G-C30-1	886.3	42.6	0.842	1.270	0.66	Rupture
3D19G-C30-2		34.0		1.095	0.77	Rupture
2D13G-C50-1	282.0	48.9	0.282	0.683	0.41	Rupture
2D13G-C50-2		34.0		0.545	0.52	Rupture
2D16G-C50-1	432.6	48.9	0.434	0.661	0.66	Rupture
2D16G-C50-2		34.0		0.528	0.82	Rupture
2D19G-C50-1	590.9	34.0	0.595	1.095	0.54	Rupture
2D19G-C50-2		34.0		1.095	0.54	Rupture
3D13G-C50-1	422.9	48.9	0.422	0.932	0.45	Rupture
3D13G-C50-2		34.0		0.744	0.57	Rupture
3D16G-C50-1	649.0	48.9	0.651	0.661	0.98	Balanced
3D16G-C50-2		34.0		0.528	1.23	Crushing
3D19G-C50-1	886.3	34.0	0.893	1.095	0.82	Rupture
3D19G-C50-2		34.0		1.095	0.82	Rupture

^aFRP rupture in case of $\rho_f < \rho_{fb}$

^bbalanced failure in case $\rho_f \approx \rho_{fb}$

^cconcrete crushing failure in case of $\rho_f > \rho_{fb}$

order to guarantee sufficient shear reinforcement against the maximum shear forces. Two longitudinal steel bars with a 9.53 mm diameter were placed in the compression zone; they served as hangers for the stirrup and provided a confinement effect along the longitudinal direction. concrete covers of 30 mm (C30) or 50 mm (C50) thickness were designed for test variables. AASHTO (2012) recommends a minimum concrete cover for unprotected main reinforcement steel to ensure durability. For the bottom of cast-in-place slabs, the concrete cover of bars up to No. 11 (36 mm diameter) should be 25.4 mm. In coastal environments, the cover should be over 75 mm. However, a GFRP bar is non-corroding reinforcement, so the concrete cover can be minimized. The minimum cover should be used if GFRP has sufficient bond strength compared with that of a conventional steel bar.

All test beams were designed in compliance with ACI 440.1R-15. Table 3 summarizes the details of the test specimens. The test specimens were designed in terms of the reinforcement ratio and effective depth. The reinforcement ratio was obtained by using different amounts of longitudinal reinforcements with measured diameters for the GFRP bars from 13.4 to 19.4 mm. For the

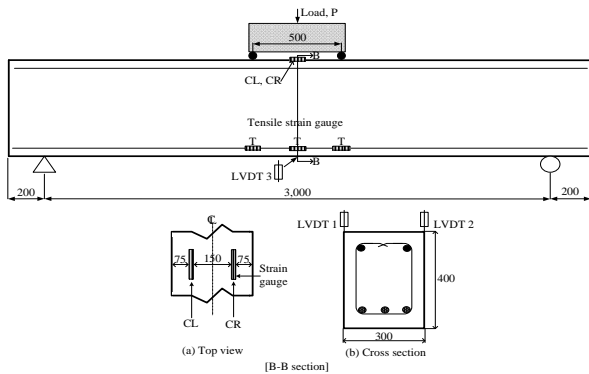


Fig. 3 Loading and measurement details (unit in mm)

effective depth, there were two depth values due to the variation in the concrete cover depth. Based on the measured concrete compressive strength, a balanced reinforcement ratio was determined. Test beams were classified in terms of three important reinforcement levels: FRP rupture, balanced, and concrete crushing failure. The designed reinforced type was investigated by using the ratio of sectional (ρ_f) to balanced (ρ_{fb}) value.

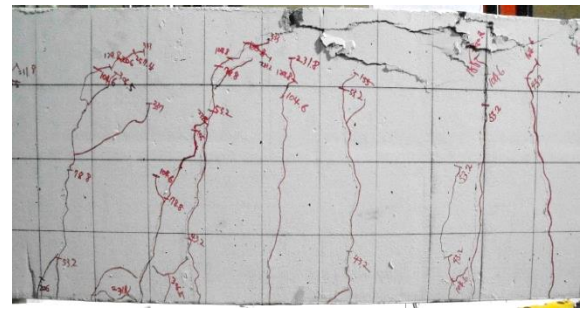
2.3 Test setup and data acquisition

A four-point loading test was carried out by using a universal test machine (UTM) with a capacity of 500 kN. Fig. 3 shows the test setup. The loading rate was divided into two sets. First, 5 kN/min was applied up to the initial cracking. Then, 12.5 kN/min was used to failure. The boundary was considered to be under the simply supported condition to ensure flexural behavior of the test beam. The clear span was 3000 mm, and the span-to-depth ratio was designed to be 3.5. The beam was subjected to pure flexure. Two specimens were considered for each test variable of the RC beams with GFRP bars. All data were collected with a data acquisition system. Loading was applied in steps of around 25 kN, and the deflection and strain were recorded. In order to measure the deflection, three linear variable differential transformers (LVDTs) were installed at the top and bottom of the test beam at the mid-section. The two LVDTs on the top checked the eccentricity of the test beam in the lateral direction. Elastic resistance strain gauges were installed in the compression and tension zones at the surface of the tensile GFRP bar and extreme top fiber of the concrete.

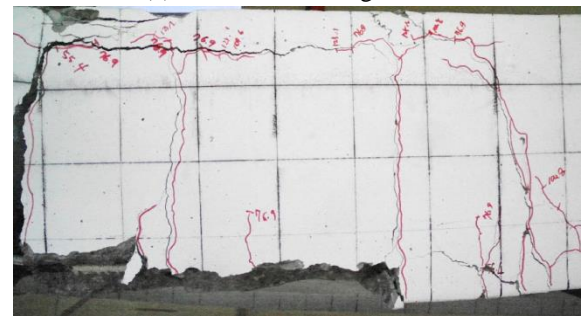
3. Test results and discussions

This section presents the most significant experimental results and their analysis. First, the mode of failure was investigated along with the flexural response, such as the load-deflection relationship, depending on the reinforcement ratio and concrete compressive strength. The effect of the effective depth from different concrete covers was examined.

3.1 Mode of failure



(a) Concrete crushing failure



(b) GFRP rupture

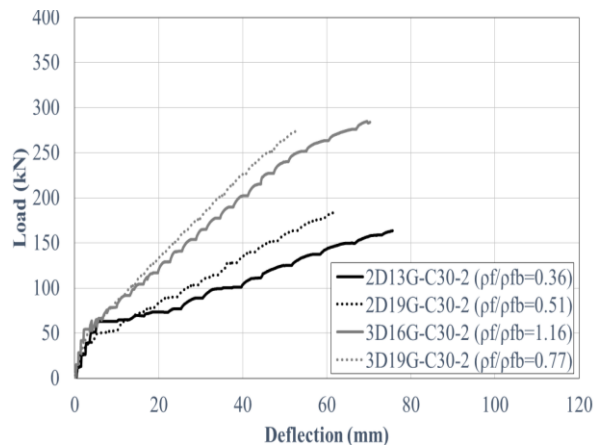
Fig. 4 Mode of failure

Two significant modes of failure were observed, as shown in Fig. 4: concrete crushing failure and GFRP rupture. These phenomena were observed in D13 and D19 reinforced specimens. According to ACI 440.1R-15, specimens that fail due to concrete crushing are less brittle than those that fail due to GFRP rupture because there is no sign of failure in the GFRP bar up to the ultimate limit state. Another mode of failure was GFRP rupture for under-reinforced D13 specimens. All specimens failed as intended according to flexural design in compliance with ACI 440.1R-15.

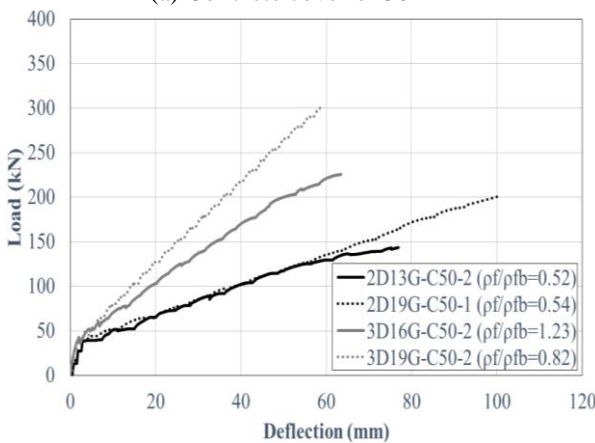
3.2 Load-deflection behavior

3.2.1 Effect of reinforcing ratio

In order to investigate the effect of the reinforcement ratio, four representative specimens designed for failure by concrete crushing and GFRP rupture were investigated. They had the same concrete compressive strength of 34.0 MPa. Fig. 5 shows the load-deflection behavior for different effective depths caused by different concrete covers. The ultimate load capacity was found to increase with the reinforcement ratio. It differed depending on whether the reinforcement ratio was higher or lower than the balanced reinforcement ratio. Around the ratio of sectional to balanced of 0.5, the load-carrying capacity greatly increased whether the concrete cover was 30 or 50 mm. This may be because the range of the reinforcement ratio was at the transition point for the mode of failure from balanced to concrete crushing. For cracking load, specimens with a concrete cover of 30 mm showed a higher cracking load than the 50 mm specimens. This is because the 30 mm specimens had a greater effective depth, so the resistance moment capacity was slightly higher than that of the 50 mm specimens.



(a) Concrete cover of 30 mm



(b) Concrete cover of 50 mm

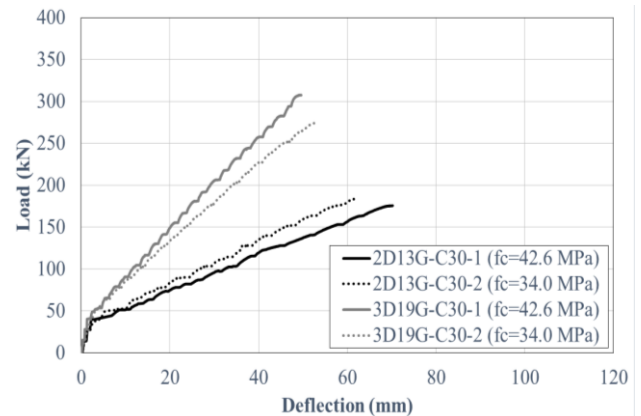
Fig. 5 Load-deflection relationship according to reinforcing ratio

3.2.2 Effect of concrete compressive strength

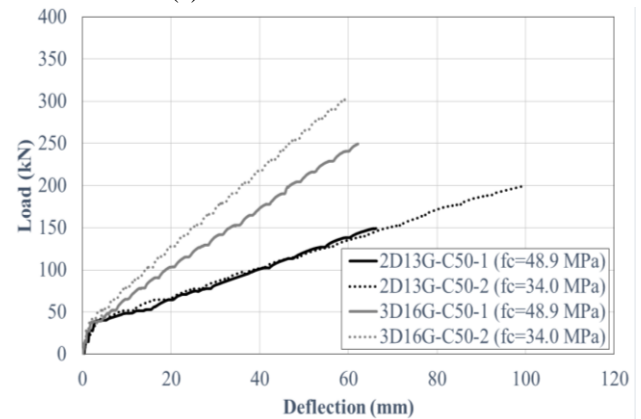
Fig. 6 shows the effect of the concrete compressive strength on the load-deflection behavior. The effect of the concrete compressive strength increasing the load-carrying capacity was investigated. This result was not common for the 2D13G-C30 specimen shown in Fig. 6(a). Specimen Nos. 1 and 2 might have shown almost the same behavior without a large discrepancy because of their low reinforcement ratios. The cracking load of specimens with a 30 mm concrete cover was slightly higher than that of the 50 mm specimens. This is the same behavior observed for the effect of the reinforcement ratio. The concrete compressive strength was found to have a much greater effect on specimens with a high reinforcement ratio rather than those with a low reinforcement ratio. This is shown in Fig. 6(b).

3.2.3 Load-strain relationship

Fig. 7 shows the relationship between the load and strain of the concrete (negative term) and GFRP bar (positive term). The analytical ultimate strain of the concrete and GFRP bar were considered to be the 0.003 and the average measured strain, respectively, in compliance with ACI 440.1R-15. The ultimate strains of D13 and D19 GFRP bars were 17,900 and 14,800 $\mu\epsilon$, respectively. The strain behavior was determined to lose elasticity after a crack



(a) Concrete cover of 30 mm



(b) Concrete cover of 50 mm

Fig. 6 Load-deflection relationship according to concrete compressive strength

opened on the bottom surface of the test beams. GFRP bars with a low reinforcement ratio showed greater creep behavior before strain hardening occurred. Increasing the reinforcement ratio reduced the creep zone, and the strain behavior transferred to strain hardening. The elastic behavior of the GFRP bar was maintained in the case of concrete crushing failure. All test specimens exhibited concrete crushing failure and GFRP rupture because they were initially designed to show the intended mode of failure.

Table 4 presents the experimental and analytical results of the test specimens. The cracking load was measured to be 48 kN for the considered test specimens, which produced a cracking moment of 30.0 kN·m. The ultimate moments of the experimental and analytical results were investigated. The theoretical value was calculated as the nominal moment strength according to the ACI 440.1R-15. For the strength limit state, the stress on the GFRP bar in tension was determined in the case of a concrete compressive strain of 0.003. The tensile strength of the GFRP bars was obtained from the uniaxial tensile test. The experimental and theoretical results showed reasonable agreement; some of the discrepancies may be due to a lack of average values for the test specimens. Once the design moment with the environmental factor is applied, the evaluated moment strength would be a conservative result, so the structural safety of the design may be ensured.

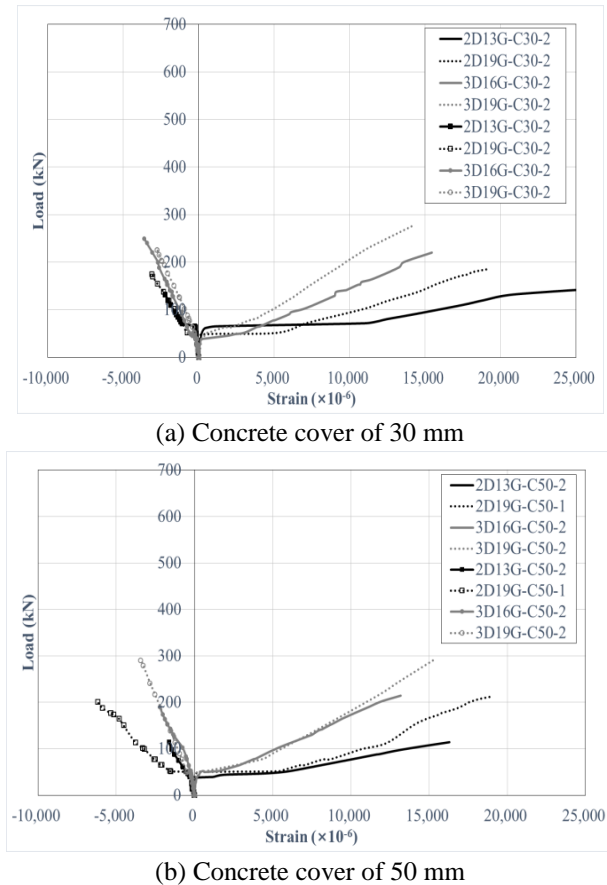


Fig. 7 Mid-span strain behavior of concrete and GFRP bar

Table 4 Ultimate moment and mode of failure of test specimens

Beam ID	Ultimate moment (kN·m)		Anal.(ACI)/Exp.	Mode of failure
	Exp.	Anal.(ACI)		
2D13G-C30-1	93.9	88.8	0.95	Rupture
2D19G-C30-1	116.6	148.1	1.27	Balanced
3D16G-C30-1	155.9	167.8	1.08	Crushing
3D19G-C30-1	171.7	177.2	1.03	Rupture
2D13G-C50-1	89.8	83.4	0.93	Rupture
2D19G-C50-1	133.5	137.2	1.03	Rupture
3D16G-C50-1	141.2	160.7	0.88	Crushing
3D19G-C50-2	188.6	161.2	0.85	Rupture

3.3 Deformability and ductility

The ductility index DI is usually applied to evaluate the ability of a steel RC beam to sustain inelastic deformations and large rotations prior to failure. This theory is not available for GFRP RC beams because they exhibit a linear response up to failure. Therefore, CSA-S6-10 (2010) specifies that the ductility of a GFRP RC beam should be evaluated according to the deformability rather than the deflection to ensure adequate deformation. Eq. (1) introduces the deformability factor DF , which consists of the moment and curvature at the service and ultimate limit states. For the service state, CSA-S6-10 recommends a

Table 5 Deformability factor, DF , for test beams using Eq. (1)

Beam ID	At service ($\epsilon_c=0.001$)			At ultimate ($\epsilon_c=0.003$)			DF
	Moment (kN·m)	C_s (mm)	Curvature (1/mm)	Moment (kN·m)	C_u (mm)	Curvature (1/mm)	
2D13G-C30-1	61.8	33.1	30.2	91.2	37.1	50.6	2.5
2D19G-C30-1	64.4	64.0	15.6	140	76.2	39.5	5.5
3D16G-C30-1	64.4	53.9	18.6	140	63.4	47.4	5.6
3D19G-C30-1	103.2	50.1	20.0	214.2	65.4	45.9	4.8
2D13G-C50-1	37.8	54.4	18.9	88.2	52.9	56.8	7.0
2D19G-C50-1	40.8	51.8	19.3	117.7	60.5	49.6	7.4
3D16G-C50-1	54.1	64.1	15.6	134.3	66.5	45.1	7.2
3D19G-C50-2	62.2	62.3	16.1	157.9	73.1	41.0	6.5

concrete compressive strain of 0.001. The value of DF should not be less than 4.0 to ensure adequate deformability of the GFRP RC beams. In this study, DF was calculated for test specimens with strain in the reinforcement. The curvature was experimentally determined by using the measured maximum and service strains.

$$DF = \frac{M_u \psi_u}{M_s \psi_s} \quad (1)$$

where,

M_u =ultimate moment (kN·m)

ψ_u =curvature at ultimate state ($\epsilon_c=0.003$, $1/C_u$)

M_s =service moment (kN·m)

ψ_s =curvature at service state ($\epsilon_c=0.001$, $1/C_s$)

C_s =distance from top fiber to neutral axis at service state

C_u =distance from top fiber to neutral axis at ultimate state

Table 5 presents the results of the calculated DF values. More reinforcement allows for lower curvatures and deformations and thus a lower DF . In addition, a lower effective depth-to-height ratio decreases DF . This phenomenon was also identified in previous results (Barris *et al.* 2009). Therefore, all beams except 2D13G-C30-1 in this study can be considered to provide acceptable deformability under the monotonic loading condition.

4. Prediction of mid span deflection

4.1 Prediction equations

The mid-span deflection of a flexural member is obtained by using the effective moment of inertia. Branson's model is a widely used analytical model of the effective moment of inertia (Branson 1965). Many design code equations for the effective moment of inertia of an RC beam with FRP bars have been modified based on Branson's model or another analytical shape with verification through experimental results. In this study, the predicted deflection of the tested beams was evaluated by using the following design code equations and the latest developed equation.

ACI 440.1R-06 (2006) recommends an equation for the effective moment of inertia based on Branson's equation. It

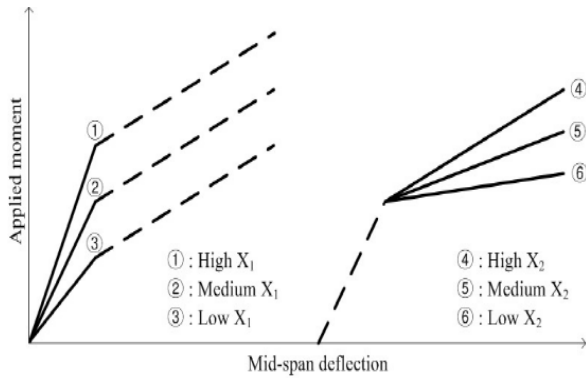


Fig. 8 Conceptual load-deflection behavior based on Adam *et al.* (2015)

has an additional factor to consider the reduced tension stiffening of an RC member with FRP. This equation is commonly used to calculate the moment of inertia of an RC member with FRP to determine the deflection of the cracked section could be calculated. It is given below in Eq. (2)

$$I_e = \left(\frac{M_{cr}}{M_a}\right)^3 \beta_d I_g + \left[1 - \left(\frac{M_{cr}}{M_a}\right)^3\right] I_{cr} \leq I_g \quad (2)$$

where, I_g =gross moment of inertia (mm^4), I_{cr} =moment of inertia of transformed cracked section (mm^4), β_d =reduction coefficient related to the reduced tension stiffening exhibited by FRP reinforced members ($=\frac{1}{5}\left(\frac{\rho_f}{\rho_{fb}}\right) \leq 1.0$), ρ_f =reinforcement ratio of GFRP bar, ρ_{fb} =balanced reinforced ratio of GFRP bar, M_{cr} =cracking moment (N·m), M_a =maximum service load moment in member (N·m).

ACI 440.1R-15 (2015) suggests a new method to determine the effective moment of inertia of an RC beam with FRP bars. This equation is based on Bischoff's proposed approach, which represents a weighted average of flexibility ($1/E_c I$) as given in Eq. (3). The equation has been reported to work equally well for RC members with both steel and GFRP without needing any empirical parameters (Bischoff 2005)

$$I_e = \frac{I_{cr}}{1 - \gamma \left(\frac{M_{cr}}{M_a}\right)^2 \left(1 - \frac{I_{cr}}{I_g}\right)} \leq I_g \quad (3)$$

where, γ =parameter to account for the variation in stiffness along the length of the member for four point bending ($\gamma = 1.72 - 0.72\left(\frac{M_{cr}}{M_a}\right)$)

CSA S806-12 (2012) suggests Eq. (4) for calculating the deflection of an RC member with FRP bars. This equation is based on the conventional equation for calculating the deflection under four-point loading. It uses the cracked moment of inertia, while ACI 440 uses the effective moment of inertia. On the other hand, additional terms representing the shear span, span length, and uncracked length for half of the beam are considered. This equation can result in a calculation-intensive process subject to human error. Therefore, the code also provides closed-form equations for common loading and support conditions.

$$\Delta = \frac{Pa}{48E_c I_{cr}} \left(3\left(\frac{a}{L}\right) - 4\left(\frac{a}{L}\right)^3 - 8\eta\left(\frac{L_g}{L}\right)^3\right) \quad (4)$$

where, P =total applied load (N), a =shear span (mm), L =span length (mm), L_g =uncracked length in half of the beam (mm) ($=a\left(\frac{M_{cr}}{M_a}\right)$), E_c =modulus of elasticity of concrete (MPa), $\eta = \left(1 - \frac{I_{cr}}{I_g}\right)$

Intelligent Sensing for Innovative Structures (ISIS 2007) recommends Eq. (5) to determine the effective moment of inertia for an RC beam with FRP bars. This equation adds additional corrective terms to a modified Branson's equation with more experimental data. The notation is the same as that introduced in the above Eqs. (2)-(4).

$$I_e = \frac{I_g I_{cr}}{I_{cr} + \left(1 - 0.5\left(\frac{M_{cr}}{M_a}\right)\right)^2 (I_g - I_{cr})} \quad (5)$$

As the latest modification, Adam *et al.* (2015) used regression analysis to reevaluate the factor β_d in Branson's equation. The two independent parameters X_1 and X_2 were determined by 3D regression analysis data fitting to be 0.227 and 0.60, respectively. This is given below in Eq. (6)

$$I_e = \left(\frac{M_{cr}}{M_a}\right)^3 \beta_d I_g + X_2 \left[1 - \left(\frac{M_{cr}}{M_a}\right)^3\right] I_{cr} \leq I_g \quad (6)$$

where, $\beta_d = X_1 \left(\frac{\rho_f}{\rho_{fb}}\right) \leq 1.0$

Eq. (6) can be divided into two parts depending on the deformation branch: before and after cracking. Coefficient X_1 governs the initial cracking load derived by the modulus of rupture of concrete from a varying concrete compressive strength. This is caused by the effect of the gross moment of inertia in the uncracked state. The coefficient X_2 governs the flexural stiffness of the second branch up to the ultimate strength; it affects the modulus of elasticity of the cracked section. Fig. 8 illustrates the conceptual load-deflection behavior depending on the coefficients X_1 and X_2 .

4.2 Analysis results and discussions for the new prediction of deflection

The aim of this study was to predict the load-deflection relationship of the representative test beams that fail due to FRP rupture and concrete crushing failure. Existing design code equations for the effective moment of inertia were considered and compared to the experimental results. A modified effective moment of inertia based on Adam *et al.*'s equation was developed and compared to the load-deflection relationships of the experimental results and other design code equations. The modification coefficients X_1 and X_2 were determined to be 0.23 and 0.7, respectively. These modifications were determined simply by considering the effect of varying X_1 and X_2 on the experimental load-deflection relationship for the uncracked and cracked branches.

In this study, the service deflection limit δ_s was taken at the moment when the concrete strain reached 0.001, as recommended by CSA-S6-10 (2010). This is equal to a

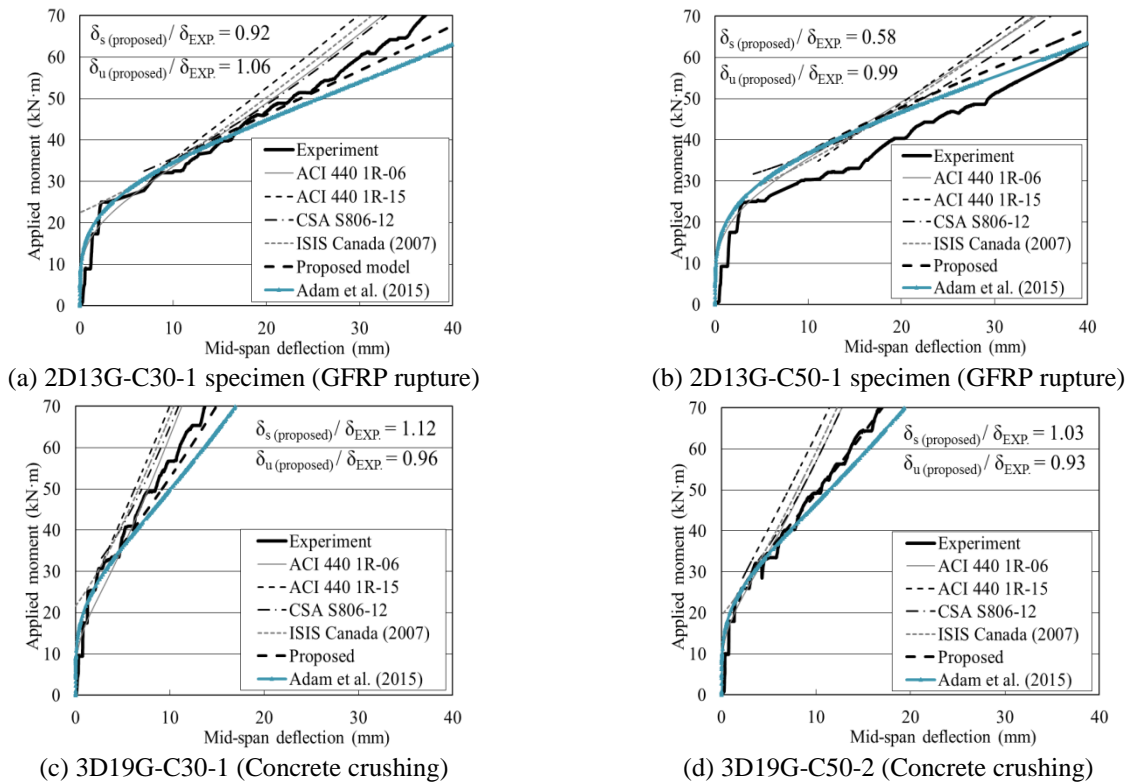


Fig. 9 Experimental vs. theoretical load-midspan deflection

value in the range of 1.1-2.2 times the cracking moment M_{cr} . The ultimate deflection limit (δ_u) was considered to be $4M_{cr}$. The deflection at the ultimate moment was applied for 2D13 specimens because the ultimate moment was lower than $4M_{cr}$. The measured and analytical deflections in the service and ultimate limit states were examined. Figs. 9(a)-(d) compare the results for the representative test beams. In general, the analysis results for all considered design code equations agreed closely with the load-deflection of the tested beams. Those predicted by ACI 440.1R-06, ACI 440.1R-15, CSA S806-12, and ISIS Canada 2007 showed reasonably good agreement with the experimental results up to the cracking moment. They then overestimated the deflection of all test beams as the applied moment was increased. ACI 440.1R-15 overestimated the most, and CSA S806-12 estimated a more conservative deflection than the other design code equations. This was due to the different uses of the effective moment of inertia. CSA S806-12 uses I_{cr} to calculate the deflection. As the applied moment is increased, I_e becomes closer to the constant value I_{cr} , where the experimental effective moment of inertia is less than I_{cr} . The analysis results showed that the proposed model predicted the deflection more accurately than the design code equations considered in this study. The deflection ratio at the service limit state was 0.92-1.12 in the experiments, except for the 2D13-C50-1 specimen. In the ultimate limit state, the ratios were 0.99-1.06. The proposed model modified based on Adam *et al.* (2015)'s equation generated much better predictions, even when the effective moment of inertia was less than the theoretical I_{cr} .

Fig. 9 proved that the proposed model could provide better predictability of the applied moment-mid span

deflection of the tested beams up to ultimate state than that of Adam *et al.* (2015). The fitting approach in this study was more effective and simply to design the structural behavior of FRP bar reinforced concrete beams.

5. Conclusions

This study experimentally investigated the flexural capacity of concrete beams reinforced with newly developed GFRP bars with an improved modulus of elasticity and bond strength. The experimental results were compared with the values obtained from design code equations and the proposed model. The conclusions are as follows:

1. The mechanical properties of the modulus of elasticity and bond strength for the new GFRP bar developed by previous study were compared with those of commercial GFRP bars. The modulus of elasticity was 26.5%-38.2% higher, and the bond strength was 42% higher. The diameter for calculating the tensile strength was measured by using an immersion test. The difference between the nominal and measured diameters was a maximum of 3.6%. The material properties were verified for application of the flexural reinforcement to concrete beams and deck slabs.

2. All of the specimens failed as intended by flexural design in compliance with ACI 440.1R-15 to verify the load-strain behavior. Increasing the reinforcement ratio greatly increased the load-carrying capacity. The concrete compressive strength was found to be much more effective for specimens with a high reinforcement ratio than those

with a low reinforcement ratio.

3. Design code equations, including ACI 440.1R-06, ACI 440.1R-15, CSA S806-12, and ISIS Canada 2007, overestimated the experimental load-deflection behavior. This may be caused by the analytical assumption that the effective moment of inertia is maintained linearly up to failure, whereas the test beam was actually governed by the cracked moment of inertia. A modified model using two coefficients was proposed and provided much better predictions, even when the effective moment of inertia was less than the theoretical I_{cr} . This result may be good extension for Adam *et al.* (2015)'s research to evaluate the structural behavior of GFRP bar reinforced concrete beams.

4. The deformability of the test beams satisfied the specified value of 4.0 in compliance with CSA S6-10. The test beams in this study provided acceptable deformability under the monotonic loading condition. Therefore, concrete beams reinforced with the newly developed GFRP bars were verified to have sufficient ductility.

Acknowledgments

This research was supported by a grant (13SCIPA01) from Smart Civil Infrastructure Research Program funded by Ministry of Land, Infrastructure and Transport (MOLIT) of Korea government and Korea Agency for Infrastructure Technology Advancement (KAIA) and Basic Science Research Program through the National Research Foundation of Korea (NRF) funded by the Ministry of Education (grant number 2016R1D1A1B03934809) and this study was supported by Kangwon National University.

References

- AASHTO (2009), *LRFD Bridge Design Guide Specifications for GFRP-Reinforced Concrete Bridge Decks and Traffic Railings*, American Association of State Highway and Transportation Officials, Washington, U.S.A.
- AASHTO (2012), *LRFD Bridge Design Guide Specifications*, American Association of State Highway and Transportation Officials, Washington, U.S.A.
- ACI 440.1R-06 (2006), *Guide for the Design and Construction of Concrete Reinforced with FRP Bars*, American Concrete Institute, Farmington Hills, U.S.A.
- ACI 440.1R-15 (2015), *Guide for the Design and Construction of Concrete Reinforced with FRP Bars*, American Concrete Institute, Farmington Hills, U.S.A.
- Adam, M.A., Said, M., Mahmoud, A.A. and Shanour, A.S. (2015), "Analytical and experimental flexural behavior of concrete beams reinforced with glass fiber reinforced polymers bars", *Constr. Build. Mater.*, **84**, 354-366.
- ASTM D 3916 (2002), *Standard Test Method for Tensile Properties of Pultruded Glass Fiber Reinforced Plastic Rods*, American Standard Test Method International, West Conshohocken, U.S.A.
- Barris, C., Torres, L.I., Turon, A., Baena, M. and Catalan, A. (2009), "An experimental study of the flexural behavior of GFRP RC beams and comparison with prediction models", *Compos. Struct.*, **91**(3), 286-295.
- Bischoff, P. (2005), "Reevaluation of deflection prediction for concrete beams reinforced with steel and fiber reinforced

- polymer bars", *J. Struct. Eng.*, **131**(1), 752-767.
- Branson, D.E. (1965), *Instantaneous and Time-Dependent Deflections of Simple and Continuous Reinforced Concrete Beams*, HPR Report No. 7, Part 1, Alabama Highway Department, Bureau of Public Roads.
- CAN/CSA S806-12 (2012), *Design and Construction of Building Structures with Fibre-Reinforced Polymers*, Canadian Standards Association/National Standard of Canada, Ontario, Canada.
- Castro, P.F. and Carino, N.J. (1998), "Tensile and nondestructive testing of FRP bars", *J. Compos. Constr.*, **2**(1), 17-27.
- CSA S6-10 (2010), *Canadian Highway Bridge Design Code*, Canadian Standards Association, Mississauga, Canada.
- FHWA (2010), *Status of the Nation's Highways, Bridges, and Transit: Conditions and Performance*, Report for Congress, Federal Highway Administration, US Department of Transportation.
- <http://www.concrete.org/students/AslanFRPREbar.pdf>
- <http://www.concrete.org/students/Pultrall-V-Rod-Technical-Data-Sheet-for-2009-Competition.pdf>
- ISIS Canada (2007), *Reinforcing Concrete Structures with Fibre Reinforced Polymers*, ISIS Canada, Winnipeg, Canada.
- Korea Expressway Corporation (2013), *Research on Decision Making Methodology for Bridge Re-Construction and Maintenance*, Report for the Korea Expressway Corporation, Expressway and Transportation Research Institute (ETRI).
- Maranan, G.B., Manalo, A.C., Benmokrane, B., Karunasena, W. and Mendis, P. (2015), "Evaluation of the flexural strength and serviceability of geopolymer concrete beams reinforced with glass-fibre-reinforced polymer (GFRP) bars", *Eng. Struct.*, **101**, 529-541.
- Park, C., Park, Y., Kim, S. and Ju, M. (2016), "New emerging surface treatment of hybrid GFRP bar for stronger durability of concrete structures", *Smart Struct. Syst.*, **17**(4), 593-610.
- Wang, H. and Belarbi, A. (2013), "Flexural durability of FRP bars embedded in fiber-reinforced-concrete", *Constr. Build. Mater.*, **44**, 541-550.
- Weber, A. (2005), "Bond properties of a newly developed composite rebar", *Proceedings of the International Symposium on Bond Behaviour of FRP in Structures (BBFS 2005)*, Hong Kong, China, December.
- You, Y.J., Kim, J.H.J., Kim, S.J. and Park, Y.H. (2015), "Methods to enhance the guaranteed tensile strength of GFRP rebar to 900 MPa with general fiber volume fraction", *Constr. Build. Mater.*, **75**, 54-62.

CC